Journal of Organometallic Chemistry, 440 (1992) 119–144
Elsevier Sequoia S.A., Lausanne
JOM 22910

Methylisocyanide derivatives of molybdenocene and tungstenocene: preparation, reactivity and electronic structure: crystal structures of $[(\eta^5\text{-}C_5H_5)_2WBr(CNMe)]Br$ and $[(\eta^5\text{-}C_5H_5)_2MoC\{N(H)CH_3\}N(H)C\{N(H)CH_3\}][BF_4]_2 \cdot CH_3CN$

Maria J. Calhorda [a], Alberto R. Dias [b], M. Teresa Duarte [b], Ana M. Martins [b], Pedro M. Matias [a] and Carlos C. Romão [a]

[a] *Centro de Tecnologia Química e Biológica, and Instituto Superior Técnico, R. da Quinta Grande, 6, 2780 Oeiras (Portugal)*
[b] *Centro de Química Estrutural, Instituto Superior Técnico, 1096 Lisboa Codex (Portugal)*

(Received March 18, 1992)

Abstract

The cationic complexes $[Cp_2MoH(CNMe)]I$ (**1**), $[Cp_2MoI(CNMe)]I$ (**2**), $[Cp_2Mo(CNMe)_2)]X_2$ (**3a**, X = I; **3b**, X = Cl; **3c**, X = PF_6) and $[Cp_2WBr(CNMe)]Br$ (**4**) are prepared from $[Cp_2MoHI]$ and $[Cp_2MX_2]$. The X-ray crystal structure of **4** shows normal end-on coordination of CNMe and no structural signs of significant metal-to-ligand back-donation. $NaBH_4$ attack on **3c** produces $[CpMo(\eta^4\text{-}C_5H_6)(CNMe)_2]PF_6$ (**5**) but CH_3O^-, PhS^-, NEt_3 and NH_3 add to the CNMe ligands to give, respectively, $[Cp_2MoC(OCH_3)N(CH_3)CNCH_3]PF_6$ (**6**), $[Cp_2Mo(CNCH_3)\{C(SPh)N(H)CH_3\}][PF_6]_2$ (**7**), $[Cp_2Mo(CNCH_3)\{C(NEt_3)NCH_3\}][PF_6]_2$ (**8**) and $[Cp_2MoC\{N(H)CH_3\}N(H)C\{N(H)CH_3\}][PF_6]_2 \cdot CH_3CN$ (**9**). Molecular orbital calculations of the extended Hückel type are used to interpret the regioselectivity of the nucleophilic attack and the bonding in the Fischer-type carbene complexes **6–9**. The crystal structure of $[Cp_2MoC\{N(H)CH_3\}N(H)C\{N(H)CH_3\}][BF_4]_2 \cdot CH_3CN$, the BF_4^- salt corresponding to **9**, is presented and the distortion observed in the metallacycle interpreted by EHMO calculations. The ylid complex $[Cp_2W(CNMe)(CHClPMe_3)]Br_2$ (**11**) is formed by reaction of **4** with PMe_3 in CH_2Cl_2. Deprotonation of **1** and Na/Hg reduction of **4** produce the d^4 electron-rich complexes $[Cp_2MCNMe]$ (**12**, M = Mo; **13**, M = W).

Introduction

Molybdenocene and tungstenocene form a wide variety of complexes with 2-electron donors, L, where the more common oxidation states of the metals are +II and +IV [1]. In the former case, very electron rich d^4 complexes $[Cp_2ML]$ (**A**) are formed, *e.g.* L = CO, olefins, acetylenes, NCR, or PR_3 [2]. The latter case is

Correspondence to: Professor C.C. Romão.

illustrated by a large number of d^2 cationic complexes, e.g., $[Cp_2MXL']^+$ (**B**) and $[Cp_2ML'_2]^{2+}$ (**C**) (L' = NH_3, amines, imines, *N*-heterocycles, PR_3, NCR, CO, olefins) [2] (Cp = η^5-C_5H_5 throughout the paper).

We have recently described the first isocyanide derivatives of all three types [3] and studied the reactions of $[Cp_2MoCNR]$ complexes with electrophiles [4].

As could have been easily predicted, the results show that the good σ-donor capability of the CNR ligand allows for favourable coordination in complexes **B** and **C** and that its good π acidity stabilizes the very electron-rich metallocene fragment in the type **C** complexes.

In previous studies on the nucleophilic attack on cationic complexes of both types **B** and **C**, we and others have shown that reaction can lead to addition, and therefore functionalization, of either the unsaturated coordinated ligand L or of the Cp rings, depending on the nature of both L and the nucleophile.

In the present paper, we describe the preparation of the novel methylisocyanide mono- and di-cations $[Cp_2M(X)CNMe]^+$ and $[Cp_2Mo(CNMe)_2]^{2+}$ and report our results on the nucleophilic addition to these complexes together with the structural characterization of $[Cp_2WBr(CNMe)]Br$ and $[Cp_2MoC\{N(H)CH_3\}N(H)C\{N(H)CH_3\}][BF_4]_2 \cdot CH_3CN$. Extended Hückel molecular orbital calculations of the bonding in the latter and related complexes were carried out. The preparation of the methylisocyanide type **A** complexes, $[Cp_2MCNMe]$ (M = Mo or W) is also reported.

Results and discussion

Preparation and characterization of the cationic complexes $[Cp_2MX(CNMe)]^+$ and $[Cp_2M(CNMe)_2]^{2+}$

The general method used for the preparation of the cationic methylisocyanide derivatives was halide substitution from the easily available starting materials $[Cp_2MHX]$ and $[Cp_2MX_2]$.

Reaction of $[Cp_2MHI]$ with CNMe in refluxing THF affords the yellow complex $[Cp_2MoH(CNMe)]I$ (**1**). In contrast with the corresponding alkyl complexes $[Cp_2MoR(CNR)]^+$ [4] no hydride insertion into the CNMe ligand is observed and, in agreement with the proposed formulation, **1** shows the expected high-field hydride resonance in the ^1H NMR spectrum at δ −8.84 ppm and ν(C≡NMe) at 2180 cm^{-1} in the IR spectrum (Table 1).

Reaction of **1** with CHI_3 gives brown crystals of $[Cp_2Mo(CNMe)]I$ (**2**) in quantitative yield. Alternatively, **2** can be prepared by reaction of $[Cp_2MoI_2]$ with 1.3 equiv. of CNMe in refluxing acetonitrile.

On the other hand, when $[Cp_2MoX_2]$ (X = I or Cl) is treated with an excess of CNMe at reflux, yellow crystals of the di-cations $[Cp_2Mo(CNMe)_2)]I_2$ (**3a**) and $[Cp_2Mo(CNMe)_2)]Cl_2$ (**3b**) separate upon cooling. The PF_6 analogue **3c** is prepared by metathetical reaction with $TlPF_6$. This kind of double halide replacement by CNR ligands has, so far, only been observed with CNMe [4]. Under the conditions used for the preparation of **3a** and **3b**, $[Cp_2WBr_2]$ gives the monocation $[Cp_2WBr(CNMe)]Br$ (**4**) quantitatively, thus reflecting the lower lability of the W complexes relative to the Mo analogues.

Table 1

Selected IR data (cm^{-1}) [a]

Compound	ν(C≡NMe)	Other peaks
1	2180s	1860w,br, ν(Mo–H)
2	2210s	
3a	2230s; 2220s	
3c	2250s; 2240s	
4	2210s; 2190sh	
5	2180s; 2150s	2780s, $\nu(C-H_{exo})$
6	1670s; 1560s	
7b	2220m; 1495s	
8b	2190s; 1550, 1480s	3480m, ν(NH)
9	1640s	3370–3490m, ν(NH)
10	1620s; 1550s	3350m, ν(NH)
11	2220s	
12 [b]	1834s	
13 [c]	1821s	

[a] KBr pellets. [b] Toluene solution. [c] Pentane solution: s, strong; m, medium; w, weak; br, broad.

The IR spectra of **1, 2, 3a, 3b**, and **3c** (KBr) (Table 1) show very strong ν(C≡NMe) absorption bands at higher wavenumbers than in the free isocyanide (2168 cm^{-1} in CH_2Cl_2 solution) indicating that back-donation from the metal is not very significant in these complexes. Similar values have been observed for other Mo^{IV} isocyanide complexes [5]. The values for the ν(C≡NMe) stretching vibration in **4** are practically the same as those observed for **2**, suggesting a very similar bonding situation for both complexes.

The ^1H NMR spectra (Table 2) show the Cp singlets in the region normally observed for this type of cationic species. In particular, the value of δ 5.98 ppm found for the Cp resonance of **3a** matches well with the values found for other di-cations, *e.g.*, the isomeric $[Cp_2Mo(NCMe)_2]^{2+}$ [8]. The CH_3 protons of the coordinated CNMe ligand (*ca.* δ 3.6 ppm) are rather deshielded when compared with the free isonitrile (δ 1.98 ppm) [6] as already observed in $[Mo(O)X(CNMe)_4]^+$ [5b].

In the ^{13}C $\{^1H\}$ NMR spectra (Table 3), the signal of the metal-bound isocyanide carbon atom is very difficult to observe due to long relaxation times and the broadening produced by the quadrupole of the nitrogen nucleus. In **3a**, this signal appears at δ 141.0 ppm (δ 156 ppm for free CNMe), consistent with an essentially σ coordination to the metal [7].

Suitable crystals of **4** were grown by slow diffusion of diethyl ether into a solution of the complex in CH_2Cl_2 and the structure was solved by X-ray diffraction analysis (see below).

Nucleophilic addition to the cations $[Cp_2Mo(CNMe)_2]^{2+}$, 3^+, and $[Cp_2WBr(CNMe)]$, 4^+

In the light of previous studies, 18-electron cations of the Cp_2M^{IV} (M = Mo or W) fragment react with nucleophiles in three different ways: (i) substitution at the metal with retention of the Cp_2M fragment [2]; (ii) addition to one of the η^5-Cp rings [8]; (iii) addition at other metal-bound unsaturated ligands [2b,9].

Table 2

^{1}H NMR data

Compound	δ (ppm) (multiplicity, relative area, $^nJ_{AX}$ (Hz), assignment)
1 [a]	5.36 (s, 10, C_5H_5); 3.57 (s, 3, CNCH_3); −8.84 (s, 1, Mo−H)
2 [b]	5.75 (s, 10, C_5H_5); 3.65 (s, 3, CNCH_3)
3a [c]	5.98 (s, 10, C_5H_5); 3.60 (s, 6, CNCH_3))
3b [d]	6.25 (s, 10, C_5H_5); 3.74 (s, 6, CNCH_3)
3c [e]	5.92 (s, 10, C_5H_5); 3.57 (s, 6, CNCH_3)
4 [f]	5.78 (s, 10, C_5H_5); 3.95 (s, 3, CNCH_3)
5 [g]	(**a**) up: 5.87 (m, 2, H_1, H_2; 5.47 (s, 10, C_5H_5); 3.97 (d, 1, $^2J_{(HH)}$ = 12.6 Hz, H_{exo}); 3.56 (s, 6, CNCH_3); 3.40 (m, 2, H_3, H_4); 2.85 (d, 1, $^2J_{(HH)}$ = 12.6 Hz, H_{endo}) (**b**) down: 5.47 (t, 2, $^2J_{(HH)}$ = 2.5 Hz, H_1, H_2); 5.32 (s, 10, C_5H_5); 3.66 (s, 6, CNCH_3); 3.24 (d, 1, $^2J_{(HH)}$ = 14.9 Hz, H_{exo}); 3.18 (d, 1, $^2J_{(HH)}$ = 14.9 Hz, H_{endo}); 2.80 (m, 2, H_3, H_4)
6 [g]	5.56 (s, 10, C_5H_5); 4.32 (s, 3, OCH_3); 3.03 (s, 3, C−N−(CH_3)−C); 2.96 (s, 3, C=NCH_3)
7b [g]	7.10–6.98 (m, 5, SC_6H_5); 5.95 (m, 1, CN(H)CH$_3$); 5.89 (s, 10, C_5H_5); 3.77 (s, 3, CNCH_3); 2.54 (d, 3, $^2J_{(HH)}$ = 4.1 Hz, CN(H)CH_3))
8a [f]	5.43 (s, 10, C_5H_5); 3.63 (s, 3, CNCH_3); 3.16 (q, 6, $^3J_{(HH)}$ = 7.4 Hz, N(CH_2CH$_3$)$_3$); 2.30 (s, 3, C(NEt$_3$)CNH_3); 1.36 (t, 9, $^3J_{(HH)}$ = 7.4 Hz, N(CH$_2$CH_3)$_3$).
8b [f]	5.77 (br, NH); 5.43 (s, 10, C_5H_5); 3.65 (s, 3, CNCH_3); 3.16 (q, 6, $^3J_{(HH)}$ = 7.4 Hz, N(CH_2CH$_3$)$_3$); 2.67 (d, 3, $^3J_{(HH)}$ = 4.6 Hz, C(NEt$_3$)N(H)CH_3); 1.36 (t, 9, $^3J_{(HH)}$ = 7.4 Hz, CN(CH$_2$CH_3)$_3$)
9 [g]	5.68 (s, 10, C_5H_5); 3.44 (br, NH); 3.16 (d, 6, $^3J_{(HH)}$ = 4.6 Hz, CN(H)CH_3)
10 [f]	8.95 (d, 1, $^2J_{(HH)}$ = 7.5 Hz, H_b or H_c, **e** or **g**); 8.86 (d, 1, $^2J_{(HH)}$ = 6.2 Hz, H_b or H_c, **e** or **g**); 8.35 (d, 1, $^2J_{(HH)}$ = 7.5 Hz, H_b or H_c, **e** or **g**); 8.26 (d, 1, $^2J_{(HH)}$ = 6.2 Hz, H_b or H_c, **e** or **g**); 7.12 (m, 1, CN(H)CH$_3$), **g** (or **e**)); 6.55 (m, 1, CN(H)CH$_3$), **e** (or **g**)); 5.52 (s, 20, C_5H_5, **e** and **g**); 3.31 (d, 3, $^3J_{(HH)}$ = 5.5 Hz, CN(H)CH_3), **e** (or **g**)); 3.22 (d, 3, $^3J_{(HH)}$ = 5.1 Hz, CN(H)CH_3), **g** (or **e**))
11 [f]	5.95 (s, 10, C_5H_5); 4.05 (s, 3, CNCH_3); 2.14 (d, 9, $^2J_{(PH)}$ = 14.6 Hz, CHClP(CH_3)$_3$); 1.50 (d, 1, $^2J_{(PH)}$ = 14.6 Hz, CHClP(CH$_3$)$_3$)
12 [h]	4.35 (s, 10, C_5H_5); 2.76 (s, 3, CNCH_3)
13 [i]	4.27 (s, 10, C_5H_5); 2.87 (s, 3, CNCH_3)

[a] CD_2Cl_2, 100 Mz. [b] CD_3CN, 100 Mz. [c] CD_3CN, 300 Mz. [d] CD_3OD, 400 Mz. [e] CD_3CN, 300 Mz. [f] CD_2Cl_2, 300 Mz, for e and g isomers see Scheme 3. [g] $(CD_3)_2CO$, 300 Mz; for a and b isomers see text; the C_5H_6 protons are numbered as H_5H_5-$CCH_3CH_2CH_1CH_4$; H_5 and $H_{5'}$ = H_{endo} and H_{exo}. [h] C_6D_6, 100 Mz. [i] C_6D_6, 300 Mz. s, singlet; d, doublet; t, triplet; q, quartet; m, multiplet; br, broad.

Table 3

^{13}C {^{1}H} NMR data

Compound	δ (ppm)
3b [a]	141.0 (CNCH$_3$); 97.3 (C_5H_5); 32.9 (CNCH$_3$)
6 [b]	218.0 (C(OMe); 159.0 (CNCH$_3$); 90.7 (C_5H_5); 66.1 (OCH$_3$); 41.9 (CNCH$_3$); 28.5 (C(C(OMe)N(CH$_3$))
8 [c]	186.7 (C(NEt$_3$); 144.4 (CNCH$_3$); 91.7 (C_5H_5); 57.8 (CN(CH$_2$CH$_3$)$_3$); 47.1 (C(NEt$_3$)NCH$_3$; 28.7 (CNCH$_3$); 17.9 (CN(CH$_2$CH$_3$)$_3$)

[a] 100.54 Mz, CD_3OD. [b] 100.54 Mz, CD_3CN. [c] 75.41 Mz, CD_2Cl_2.

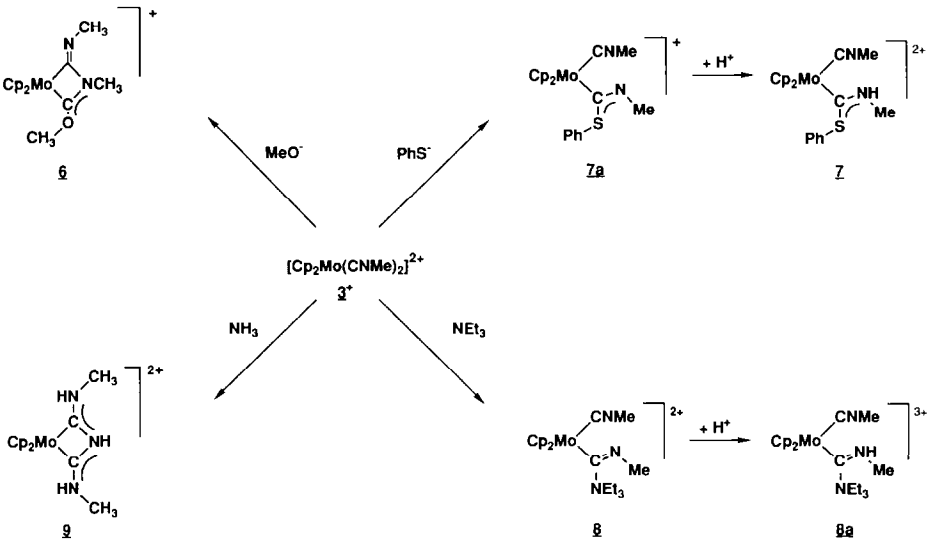

Scheme 1. Addition of nucleophiles at the CNMe in $[Cp_2Mo(CNMe)_2]^{2+}$ ($\mathbf{3}^+$).

Since the type of regioselectivity observed may depend on the nature of the nucleophile, we set out to study the reactions of $\mathbf{3}^+$ and $\mathbf{4}^+$ cations with neutral (NH_3, NEt_3, and PMe_3) and negatively charged nucleophiles (RO^-, RS^-, and H^-). The products obtained by nucleophilic addition to $\mathbf{3}^+$ are shown in **a**, **b** and Scheme 1 and are fully characterized, analytically and spectroscopically, except for **7** and **8a** which could only be spectroscopically characterized.

Treatment of a solution of $[Cp_2Mo(CNMe)_2)][PF_6]_2$ (**3c**) in acetonitrile, with 1 molar equiv. of $NaBH_4$ followed by removal of the solvent, extraction of the residue into CH_2Cl_2, concentration and addition of Et_2O, gives an excellent yield of yellow crystals of the complex formulated as $[CpMo(\eta^4\text{-}C_5H_6)(CNMe)_2]PF_6$ (**5**). From the spectroscopic data, it is immediately recognizable that H^- addition to one of the Cp rings had taken place.

Indeed, the IR spectrum of **5** shows two bands assignable to ν(C≡NMe) stretching vibrations at 2180 and 2150 cm^{-1} and a strong band at 2780 cm^{-1} which is characteristic of the exo C-H vibration of the methylene group of the $\eta^4\text{-}C_5H_6$ ligand [8,10]. The ^1H NMR spectrum of **5**, at room temperature, shows two broad signals at δ 5.62 and 3.09 ppm together with peaks assignable to η^5-Cp and CNMe. Upon cooling to −50°C the first broad peaks resolve into two signals each, and the whole spectrum corresponds to a mixture of two isomers, of structures **a** and **b**.

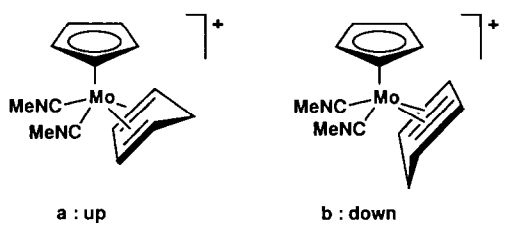

The ratio of the isomers, as measured by the ratio of the corresponding η^5-Cp singlets, is 1 : 1.7. Careful integration allowed identification of the signals for both isomers, assigned with the help of reported data on similar complexes [11] and of double resonance experiments, as summarized in Table 2.

The relatively high difference in the chemical shifts of the two doublets of the AB spin system of the methylenic protons of the η^4-C_5H_6 ligand in isomer **a** suggests its assignment as the "up" conformation. Conversely, the "down" isomer **b**, where both the *exo* and *endo* protons of the methylenic group do not suffer such a different influence of the η^5-Cp ring current, shows a much smaller difference in the chemical shifts of these protons (0.06 ppm). This type of assignment has been made for the isostructural complexes $[CpMo(\eta^4\text{-}C_5H_6)R(CO)]$ [11] and also for the analogues $[CpMo(\eta^4\text{-}C_5H_6)(CO)_2]^+$ [12] and $[CpMo(\eta^4\text{-}C_5H_6)dppe]^{2+}$ [8,12]; the latter is only known as the structurally characterized "up" isomer, fluxional at room temperature.

From the point of view of the regioselectivity predictions based on a perturbation theory and admitting charge-control on addition of negatively charged nucleophiles to 18-electron cations, H^- addition to $\mathbf{3}^+$ was expected to take place at one of the CNMe ligands. Indeed, EHMO calculations [13] on the di-cation $[Cp_2Mo(CNMe)_2)]^{2+}$ ($\mathbf{3}^{2+}$), suggest a charge of +0.224 for the *C*NMe atom which is much higher than the highest charged *C* atom in the rings (−0.027) (**c**).

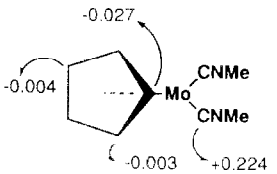

c

On the other hand, assuming that the reaction is orbitally controlled, a different result might be expected. The LUMO of the complex has significant contributions not only from the *C*NMe atom (~ 8%), but also from the η^5-Cp ring (to a total of ~ 15%), as can be seen in **d**.

Both sites may thus compete for the nucleophile, the ring being more available on steric grounds than the isonitrile. Of course, we cannot rule out the possibility that **5** corresponds to the thermodynamically and not the kinetically controlled reaction product.

The di-cation **3c** does not react with ethanol or methanol even in refluxing acetonitrile but gives untractable mixtures when treated with the corresponding sodium alkoxides in the same solvent. However, in a mixture of acetonitrile/methanol as solvent, **3c** reacts with 1 molar equiv. of NaOMe to give the metallacyclic adduct $[Cp_2MoC(OCH_3)N(CH_3)CNCH_3]PF_6$ (**6**). No ν(C≡NMe) vibrations are observed in the IR spectrum of **6**. Instead, strong peaks at much lower wavenumbers are observed and assigned to ν(C=N) vibrations, both terminal (1670 cm^{-1}) and endocylic (1560 cm^{-1}), consistent with reported values for similar compounds [14]. The ^1H NMR spectrum of **6** shows four singlets at δ 5.56 (η^5-Cp), 4.32 (OCH_3), 3.03 (C–N(CH_3)–C) and 2.96 ppm (C=NCH_3). The two higher field resonances, being broader than the first two, are assigned to *N*-bound methyls. Consistent with reported observations, the broader of these two resonances is

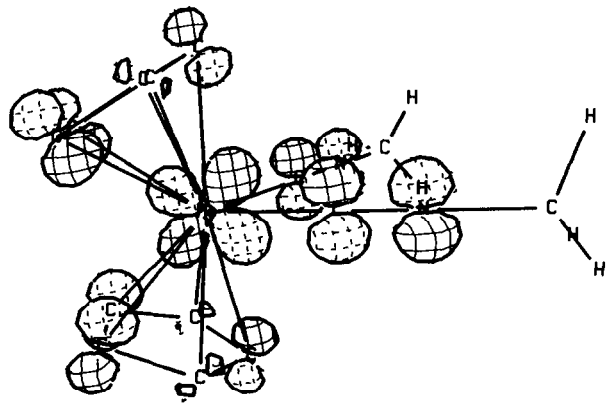

x
z
y

d

assigned to C=N(CH_3), where the influence of the nitrogen quadrupole is most strongly felt on the adjacent protons [15].

In the ^{13}C {^1H} NMR spectrum, the resonance assignable to the metal-bound carbenoid ligand is at δ 218 ppm (Mo*C*(OMe)N). The other metal-bound carbon atom is less shielded (δ 159.0 ppm) and all the other carbon signals are assigned on the basis of their chemical shifts [16]. Hindered rotation about the exocyclic C=N and C–OMe bonds could give rise to four isomers. However, only one isomer is present, as shown by ^1H NMR spectroscopy. ^1H NOESY experiments show the proximity of the two N–CH_3 groups and no signs of OCH_3–NCH_3 interaction, supporting the structure proposed in Scheme 1.

Reaction of **3b** with [Et_4N]SPh, in acetonitrile leads to the formation of a new product, [Cp_2Mo(CNCH$_3$){C(SPh)N(H)CH$_3$}][PF_6]$_2$ (**7**) which we cannot purify due to incomplete separation of $[Et_4N]^+$ salts. However, its structure was established with spectroscopic data and is shown in Scheme 1. The ^1H NMR spectrum of **7**, in Me_2CO-d_6 shows, besides the expected resonances for η^5-Cp, Ph and CNMe protons, a doublet at δ 2.54 ppm and a multiplet at δ 5.95 ppm ($^3J_{(HH)}$ = 4.1 Hz) readily assigned to a C=N(*H*)CH_3 group. The magnetic equivalence of both η^5-Cp rings indicates that the –C(SPh)=N(H)CH$_3$ ligand lies on the plane bisecting the Cp–Mo–Cp angle, which also contains the CNMe and the Mo atom. This is in agreement with the theoretical predictions discussed below. The expected ν(C≡NMe) is at 2220 cm^{-1}, with a strong peak at 1495 cm^{-1} assignable to ν(C=N). N–H stretching vibrations are present in the IR spectrum, as a consequence of the facile protonation of the thioiminoacyl ligand initially formed in adduct **7a** in the presence of residual water. The structure presented in Scheme 1 provides, as judged by molecular models, the least sterically hindered ligand arrangement in the N=C–Mo–C(S)N plane. At this stage nothing can be said to explain the absence of cyclization in **7a** in a fashion analogous to that found for **6**. However, as pointed out by Cooper [17], the factors controlling the formation of metallocycles [Cp_2W(C(S)N(R)CO)] (R = Me, Ph) are quite subtle.

The next reactions pose the same problem, since non-cyclized adducts, **8** and cyclized adducts, **9** are obtained with NEt_3 and NH_3, respectively. When the orange compound resulting from NEt_3 addition to **3c** in dry NCMe is taken up in strictly anhydrous CD_2Cl_2, the ^1H and ^{13}C $\{^1H\}$ NMR spectra are entirely consistent with the formulation $[Cp_2Mo(CNCH_3)\{C(NEt_3)NCH_3\}][PF_6]_2$ (**8**). The most deshielded resonance in the ^{13}C $\{^1H\}$ NMR spectrum is assigned to the metal-bound iminoyl carbon Mo–$C(NEt_3)$NMe. Again, the planarity of the N–C–Mo–$C(NEt_3)$N ligand is implied by the presence of only one η^5-Cp resonance. Addition of a small amount of water to the ^1H NMR sample in CD_2Cl_2 leads to the tri-cation, **8a**, with the $=N(H)CH_3$ resonances appearing as a doublet ($NHCH_3$) and a quartet ($NHCH_3$), as confirmed by double-resonance experiments.

The IR spectrum of pure **8** cannot be obtained in KBr pellets due to rapid protonation by air moisture. The peaks expected for **8a** are, however, present, namely ν(N–H) at 3480 and ν(C≡NMe) at 2190 cm^{-1}.

Treatment of **3a** with gaseous NH_3 in NCMe solution followed by counter-ion metathesis with $TlPF_6$ and recrystallization from $NCMe/Et_2O$, gives the orange cyclized adduct $[Cp_2Mo\overline{C\{N(H)CH_3\}N(H)C}\{N(H)CH_3\}][PF_6]_2 \cdot CH_3CN$ (**9**). Strong N–H bands are present in the IR spectrum, together with strong ν(C=N) peaks at *ca.* 1560 cm^{-1}. The ^1H NMR spectrum in Me_2CO-d_6 at −60°C shows only one η^5-Cp resonance and only one $=NCH_3$ doublet, at δ 3.16 ppm with $^3J_{(HH)} = 4.6$ Hz and integrating for 6 H. The expected quartet for $=NH$ is too broad to be observed. However, a broad resonance at δ 3.44 ppm is assignable to the central NH. These observations suggest that the bidentate ligand is both planar and symmetrical, with delocalized bonds. A crystal structure determination of **9** as the BF_4^- salt, prepared by addition of $TlBF_4$ instead of $TlPF_6$ and recrystallized from $NCMe/Et_2O$, confirms the planarity of the chelating ring but shows asymmetry in the ligand, as discussed below.

The proposed mechanism for the formation of **9** is depicted in Scheme 2. After the NH_3 addition to **3a**, proton rearrangement takes place leaving the strongly nucleophilic NH_2 group free for further attack on the adjacent CNMe ligand. A similar proton migration leads to the final product. Similar cyclizations have been reported for NH_2Me addition to octahedral isocyanides of Fe^{II} [18], Ru^{II} [19] and Rh^{II} [20].

Evidence for the first step of this mechanism is provided by the addition of NH_3 to $[Cp_2WBr(CNMe)]Br$ (**4**). Under conditions similar to the ones used in the preparation of **9**, **4** reacts with NH_3 in NCMe to give a brown complex formulated as $[Cp_2WBr\{C(NH_2)N(H)CH_3\}]Br$ (**10**). Of the four possible isomers of this complex shown in Scheme 3, only two are observed by ^1H NMR spectroscopy at −80°C.

Two distinct NCH_3 signals appear as doublets at δ 3.22 and 3.31 ppm, in a 1 : 1 ratio. The corresponding NH multiplets appear at δ 7.12 and 6.55 ppm, respectively. As discussed in the Molecular Orbital studies section (see below), isomers **f** and **h** are disfavoured with respect to **e** and **g** due to steric repulsions with the adjacent ligands (Cp and Br, respectively). However, the latter two are equally stable and have a relatively low barrier of rotation around the M–C bond which allows interconversion (see Fig. 4). Furthermore, the most stable plane for the ligand is perpendicular to the plane defined by the normals to the M–Cp rings and is therefore coplanar with W and Br. This easily fits with the 1 : 1 ratio for the two

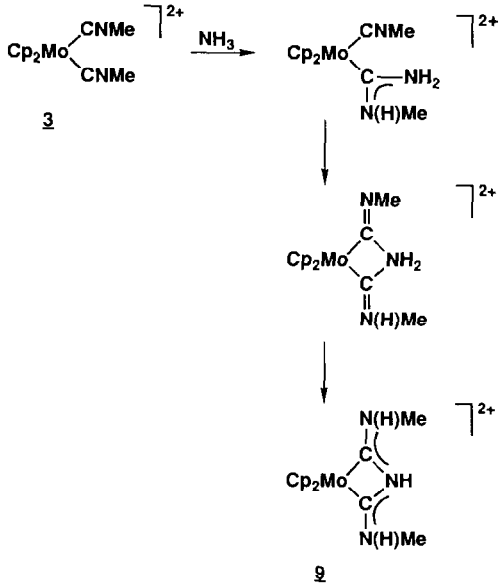

Scheme 2. Proposed mechanism for the formation of **9**.

isomers and also with the equivalence of the two η^5-Cp rings observed in the ^{1}H NMR spectrum. The assigment of signals to the isomers (rotamers) **e** and **g** was not attempted.

A totally different product is obtained by reaction of **4** with an excess of PMe_3 in CH_2Cl_2. Work-up of the reaction mixture allowed the separation of $[CH_2ClPMe_3]Cl$, identified by ^{1}H NMR spectroscopy, and an orange crystalline compound, $[Cp_2W(CNMe)(CHClPMe_3)]Br_2$ (**11**). The IR spectrum of **11** shows that no addition takes place at the CNMe since the ν(C≡NMe) peak at 2220 cm^{-1} is present. ^{1}H NMR spectroscopy shows the η^5-Cp and $CNCH_3$ singlets, together

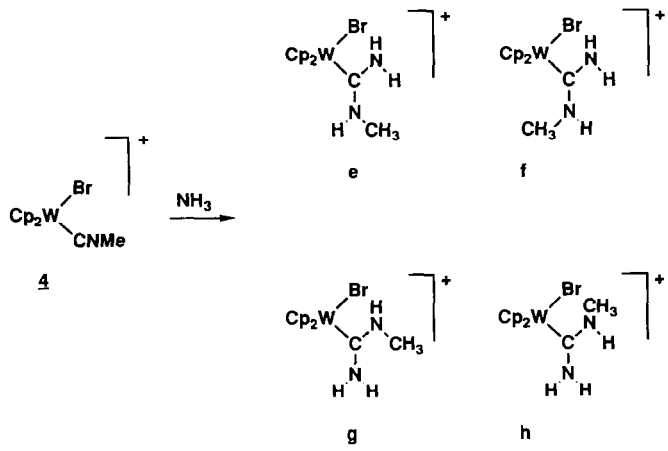

Scheme 3. Possible isomers of **10**.

with doublets at δ 2.14 and 1.15 ppm. The coupling constants of these doublets is the same (14.6 Hz) and can be attributed to coupling with the ^{31}P nucleus. The formation of chloromethylphosphonium suggests the intermediacy of the Me_3PCHCl ylide, which then replaces bromide leading to **11**.

Preparation of [Cp_2MCNMe] (M = Mo, W)

Treatment of a suspension of [$Cp_2Mo(H)CNMe$]I (**1**), with NaH in THF gives a brown solution. After filtration and evaporation to dryness, the residue was sublimed to give highly air sensitive crystals of [$Cp_2MoCNMe$] (**12**) in *ca.* 40% yield. In agreement with the observations made for the analogous CNEt and CN^tBu derivatives, the ^1H NMR spectrum shows a rather low chemical shift for the η^5-Cp rings at δ 4.35 ppm, and the IR spectrum in toluene solution shows an intense absorption for ν(C≡NMe) at 1834 cm^{-1}, implying very extensive back-donation from the metal to the CNMe. The structural studies on the [Cp_2MoCN^tBu] analogue and the theoretical studies on **12** clearly show this to be the case [4].

The corresponding W complex, [Cp_2WCNMe] (**13**), can be prepared by Na/Hg reductive dehalogenation of **4**, and again isolated by vacuum sublimation. As expected, **13** has a rather low value for ν(C≡NMe), 1821 cm^{-1} (pentane solution). For both **12** and **13**, the yields are modest and irreproducible being 40% in the most favourable case. However, use of alternative methods and/or carefully controlled conditions as reported for the preparation of the CNEt and CN^tBu derivatives [4] will certainly provide better yields.

Crystallographic and molecular orbital studies

Crystal structure of [$Cp_2WBr(CNMe)$]Br (4). Two independent cations and two independent anions are found in the asymmetric unit. A PEANUT plot [21] of cation 1 of the complex, along with the atom numbering scheme is shown in Fig. 1. As can

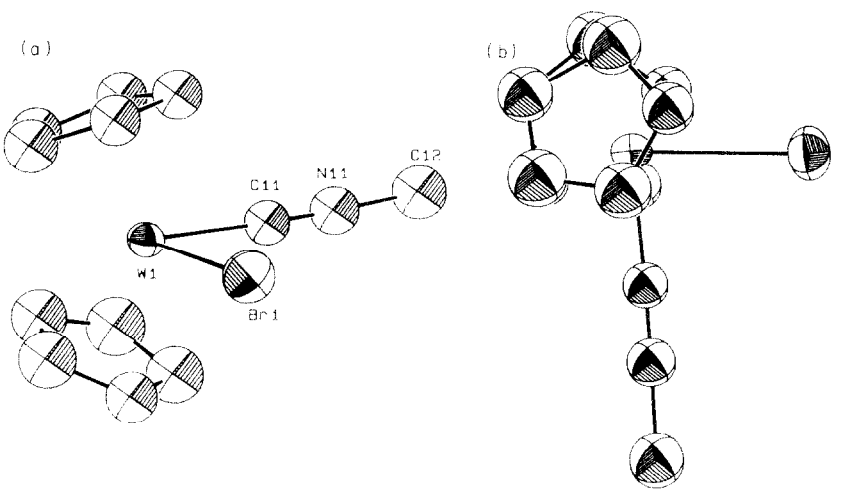

Fig. 1. Molecular diagram of cation 1, with ellipsoids at 40% probability level, of [$Cp_2W(Br)CNMe$]Br (**4**): (a) perspective view; (b) projection on the W–Br–C plane.

Table 4

Selected bond lengths (Å) and angles (°) for $[Cp_2W(Br)CNMe]Br$ (**4**)

Br1–W1	2.612(6)	Cp1–W1–Cp2	139(2)
Br2–W2	2.613(6)	C11–W1–Br1	83.3(7)
Cp1–W1	1.96(4)	N11–C11–W1	178(2)
Cp3–W2	1.96(4)	C12–N11–C11	178(3)
N11–C11	1.14(3)	Cp3–W2–Cp4	138(2)
N21–C21	1.16(3)	C21–W2–Br2	82.0(8)
C11–W1	2.012(28)	N21–W2–C21	177(2)
C21–W2	2.019(27)	C22–N21–C21	175(2)
Cp2–W1	1.97(4)		
Cp3–W2	1.98(4)		
C12–N11	1.45(3)		
C22–N21	1.49(3		

be seen from the selected bond lengths and angles presented in Table 4, the two cations have a very similar molecular geometry.

The W atom is coordinated to two η^5-Cp rings, a C atom of the CNMe (L) and to a Br atom in a pseudo-tetrahedral environment, as found in other $[Cp_2MXL]^+$ complexes [22]. The MXL fragment defined by the atoms W, Br, C1, N and C2 is planar (maximum deviations of ± 0.025 Å) and practically bisects the Cp–W–Cp angle. This angle, defined as between the normals to the least squares planes of the η^5-Cp rings, is 139(2)° and 138(2)° for each cation, with C–W–Br angles of 83.3(6)° and 82.0(7)°, respectively. Both angles are, therefore, typical of $[Cp_2MXL]^+$ complexes. The W–C–N–C bonds are almost linear. The C1–N bond lengths (1.14(3) and 1.16(3) Å) are characteristic of a C–N triple bond as in the complex $[MoCl(O)(CNMe)_4]I_3$ [23]. The W–C distances of 2.01(3) and 2.02(3) Å are rather short when compared to other W–isocyanide bonding distances, which have an average value of 2.10(3) Å [24], or to the values observed in complexes of the type $[(\mu\text{-H})W_2(CO)_7(MeNC)_2(NO)]$ [25] that vary from 2.17(2) to 2.19(2) Å, but are similar to the value found in $[W(S^iPr)(CN^tBu)\{\eta^2\text{-}C_4(CF_3)_4CN^tBu\}Cp]$ [26] of 2.017(9) Å. The W–Br distance is well within the range of values for this bond [24].

The coordination geometry, with the W–Cp distances of 1.95(4), 1.97(4), 1.98(4), and 1.96(4) Å is comparable to those in the acetonitrile complex $[Cp_2Mo(I)NCMe][PF_6]$ [2], where N–Mo–I = 81.2(1)°, Cp–Mo–Cp = 133.8(3)°, Mo–Cp = 1.986(8), 1.96(1) Å and Mo–I = 2.832(4) Å. A projection on the W–Br–C1 plane shows that the Cp rings adopt an eclipsed conformation (Fig. 1b).

Crystal structure of $[Cp_2Mo\overline{C\{N(H)CH_3\}N(H)C\{N(H)CH_3\}}][BF_4]_2 \cdot CH_3CN$ *(**9**).* Figure 2 shows a PEANUT plot [21] and the atom numbering scheme of the cation in two different views. Some bond angles and distances are shown in Table 5.

One independent cation, two anions and one solvent molecule are found in the asymmetric unit. The coordination geometry of the cation is again pseudo-tetrahedral, with the Mo atom coordinating to the two η^5-Cp rings and two carbon atoms of the MeN(H)CN(H)CN(H)Me. The ML moiety bisects the Cp–Mo–Cp angle. Although not shown in Table 5, the angle between the normals to the η^5-Cp rings, 142(2)°, is one of the largest found so far for bent metallocene complexes of Mo comparable to 145.8° in $[Cp_2MoH_2]$ [27], 144.6° in $[Cp_2MoH(SnMe_2Cl)]$,

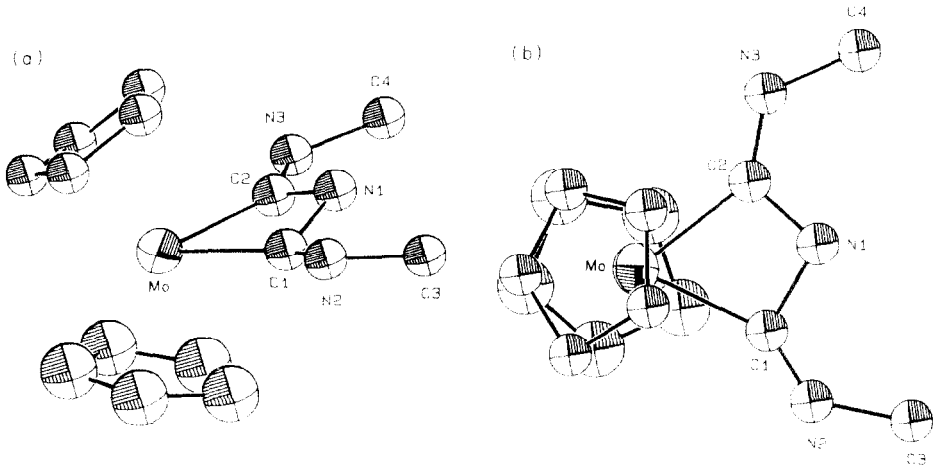

Fig. 2. Molecular diagram of the cation $[Cp_2MoC\{N(H)CH_3\}N(H)C\{N(H)CH_3\}]^{2+}$ in **9**, with ellipsoids at 40% probability level: (a) perspective view; (b) projection on the Mo–C1–C2 plane.

146.1° in $[Cp_2MoH(SnMe_3)]$ [28] and 147.7° in $[Cp_2MoCN^tBu]$ [4; and refs. cited therein]. The C1–Mo–C2 angle, 63.4(9)°, apparently small for a L–Mo–L angle in these systems, is, however, quite common for bent metallocenes coordinated to ligands forming four-membered rings.

This can be seen, for instance, in the complexes $[Cp_2Mo(2\text{-}NHNC_5H_4)]PF_6$ [29], $[Cp_2Mo(2\text{-}OHNC_5H_4)]PF_6$ [29], $[Cp_2Mo\{\eta^2\text{-}(O,N)\text{-}OC(O)NPh\}]$ [30], $[Cp_2Mo(2\text{-}SNC_5H_4)]$ [31] and $[Cp_2Mo(SO_4)]$ [32], with angles 59.8(3), 61.2(4), 61.9(1), 64.9(2) and 66.1(2)°, respectively, and results from the balance between making strong metal–ligand bonds without deforming the strained ligand too much, as was discussed earlier [29].

The Mo–C bonding distances, 2.14(2) and 2.12(2) Å, can be compared to the values found in $[Cp_2Mo(CN)_2]$, 2.124(7) and 2.125(7) Å [33]. The values are also very similar to the metal–carbon bond lengths in coordinated isocyanides (average of 2.11(3) Å [24]) and alkynes (values ranging from 2.03(5) to 2.08(3) Å [24]) and, as expected, rather short when compared to Mo–alkyls, such as 2.268(4), 2.272(4) Å in $[Cp_2Mo(^nBu)_2]$ [34] and 2.269(7) Å in $[Cp_2Mo(CH_3)(PPh_3)PF_6$ [35].

Table 5

Selected bond lengths (Å) and angles (°) for **9**

C1–Mo	2.14(2)	C2–Mo–C1	63.4(9)
C2–Mo	2.13(2)	C2–N1–C1	100(1)
C1–N1	1.53(2)	C3–N2–C1	133(2)
C2–N1	1.38(2)	C4–N3–C2	125(2)
C1–N2	1.20(2)	N2–C1–N1	116(1)
C3–N2	1.51(3)	N3–C2–N1	120(2)
C2–N3	1.34(2)	N1–C1–Mo	94.2(9)
C4–N3	1.52(2)	N2–C1–Mo	148(2)
Cp1–Mo	1.98(3)	N1–C2–Mo	100(1)
Cp2–Mo	1.93(3)	N3–C2–Mo	138(2)

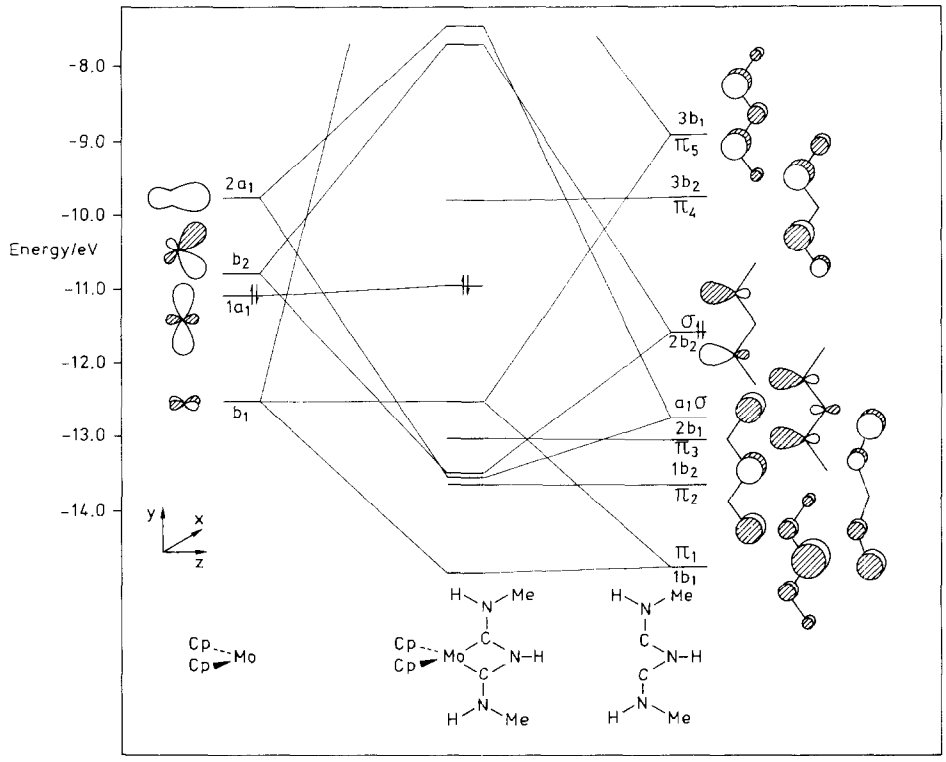

Fig. 3. Molecular orbital diagram showing the interaction between the fragments Cp_2Mo^{2+} and the ligand MeN(H)CN(H)CN(H)Me.

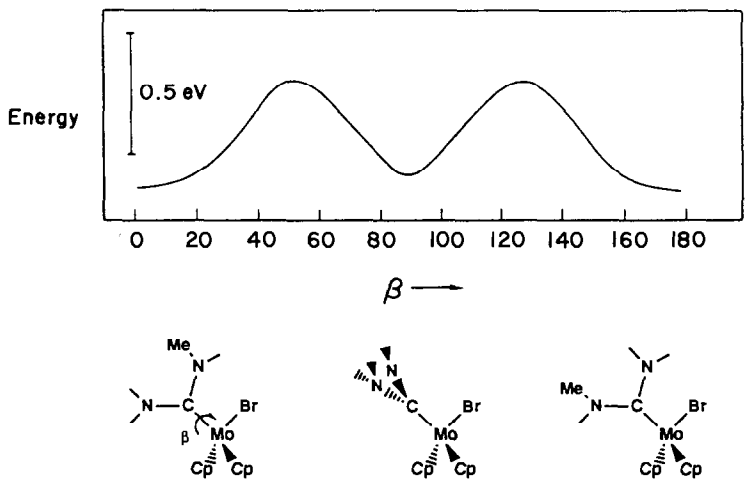

Fig. 4. Total energy dependence on the rotation of the ligand $NH_2CN(H)Me$ around the Mo–C bond.

The ligand is almost planar, the atoms MoN1C1N2C2N3 lying in a plane with maximum deviations of ±0.054 Å. The other carbon atoms, C3 and C4, are 0.23 Å and 0.07 Å away from that plane. An asymmetric bond localization is found in the N1C1N2C2N3 skeleton of the ligand in **9**. In fact, the N1–N2 and N3–C2 distances, 1.38(2) and 1.34(2) Å, suggest delocalized double bonds, while N1–C1, 1.54(2) Å, is a single bond and C1–N2, 1.23(2) Å, is close to a triple bond. This asymmetry is also reflected in the angles around the C1, C2, N2 and N3 (see Table 5).

Molecular orbital calculations on 9 and related complexes. Extended Hückel molecular orbital calculations were performed in order to understand the structure of the ligand. It is useful, however, to look first at the bond lengths in a very similar ligand coordinated to iron in a rather different environment, $[Fe(CNMe)_4\{C(NHMe)N(Me)C(NHMe)\}]^{2+}$ [18b]. They are shown, side by side, with those of **9** in **i**.

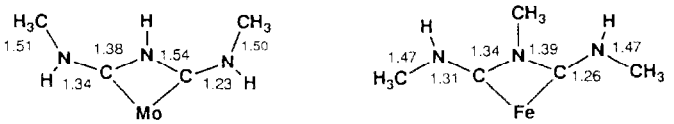

i

Although the ligand asymmetry is not present in the Fe complex, an alternation of stronger (outer) N–C bonds and weaker (inner) N–C bonds is also observed. The left ends of the ligands are very similar.

An idealized model, assuming all C–N bonds to be 1.46 Å and all the others very close to the experimental value, and C_{2v} symmetry, was used in the calculations (Experimental section). Under these conditions, overlap populations which scale as bond strengths can be used to predict which bonds should be stronger, leading to shorter bonds in the real molecule. The results for the Fe and the Mo complexes are given in **j** and are very comparable. Notice the antibonding interaction between the metal and the central N of the ligand.

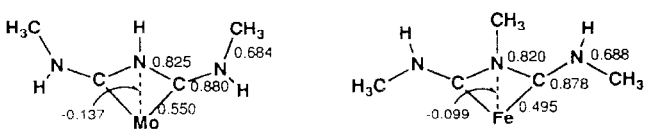

j

A molecular orbital diagram showing the interaction between the C(NHMe)N(H)C(NHMe) ligand and the $MoCp_2$ fragment is given in Fig. 3. On the left are the three well known frontier orbitals of the bent metallocene [36a] together with a group of others which, surprisingly, play only a small role in the bonding in this complex. The five π orbitals of the "pentadienyl-like" ligand and the two linear combinations of the carbon lone pairs (a_1, b_2) are shown on the right hand side. Besides the expected ligand-to-metal electron donation (from a_1, b_2 to $1a_1$, b_2), resulting in the formation of two strong Mo–C σ bonds, there is also a small back donation component [36a]. This has rarely been observed in

Cp_2Mo^{IV} derivatives such as $[Cp_2Mo(CN)_2]$. The π orbital involved in this interaction is strongly antibonding between the central N and the adjacent carbon and its population leads to weakening of this inner C–N bond. A reinforcement of this effect comes from depopulating the a_1 σ orbital, which is bonding inside the ligand skeleton. The resulting molecular orbital has bonding character between Mo and C, as expected, but due to its symmetry, it is antibonding between Mo and the central N, and responsible for the repulsion reflected in the respective overlap population, **k**.

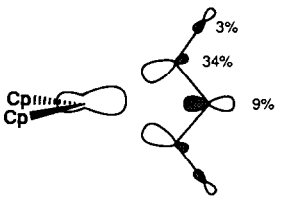

k

The bonding pattern is similar in the Fe complex. It differs from the Mo complex essentially in the different arrangement of the methyl groups at the outer N atoms of the ligand, which are respectively *cis* (Fe) and *trans* (Mo). Calculations showed these conformations to be the most stable in each case, the preference for the *cis* form becoming stronger (1.2 eV more stable) when a methyl group replaces hydrogen at the central nitrogen. The energy differences are small and the preferences can be understood on steric grounds. The intra-ligand repulsions are stronger in the *trans* form as shown in **l** and they determine the geometry of the octahedral Fe complex, where the other two ligands in the same plane are the sterically non-demanding CNMe.

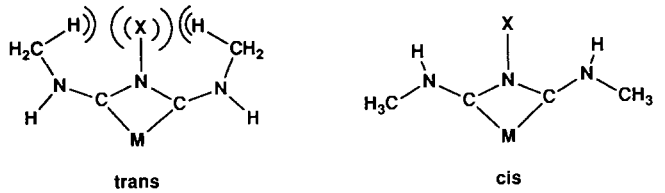

l

On the Mo complex, however, the metal coordination sphere contains two bent Cp groups. A *cis* arrangement leads to strong Me–Cp repulsions, so that the *trans* is preferred. This balance between different types of ligand–ligand repulsion has been observed for other Cp_2M complexes and discussed before [37].

Nothing in the molecular orbital diagram shown in Fig. 3 suggests a distortion in the Mo complex. There is a relatively large HOMO-LUMO gap. In an attempt to find a reason for the asymmetry of the ligand, a fluoride was allowed to approach one of the hydrogens attached to nitrogen, to probe the effect of hydrogen bonds in the crystal structure. The major result was a decrease in overlap population of the inner N–C bond and an increase in overlap population for the outer N–C bond (which in the real structure approach a single and a triple bond respectively). Other bonds also change a little, suggesting that BF_4^- anions closer to one NH group than to the other may be responsible for the observed distortion.

The crystal structure reveals that several F atoms of the BF_4^- anions are close to all NH groups and formation of hydrogen bonds may take place. The acetonitrile molecule, however, is near the less distorted side of the cation, N3 in Fig. 2, which suggests that the nitrogen on the other side of the molecule, N2, is more likely to be involved in more hydrogen bonds. This should lead to the observed distortion. The behaviour in solution is in agreement with this: the equivalence of the two CH_3 groups in the ^1H NMR spectrum in solution implies either a fast dynamic equilibrium between the two bond-localized asymmetric isomers or a symmetrical structure.

Molecular orbital calculations on the carbene derivatives. Two complexes containing the ligand C(NHMe)X (X = SPh or NH_2) were obtained following nucleophilic attack at the carbon atom of coordinated isonitrile but no structure determinations were possible.

For a CR_2 type carbene (R = alkyl), the M–C bond interactions would be maximized with the CR_2 plane lying perpendicular to the plane containing M, C, and the adjacent ligand, **m**, as the frontier orbitals of MCp_2 also lie on this plane (see Fig. 3) [36b].

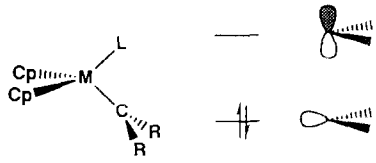

m

The frontier orbitals of carbene ligands containing heteroatoms are different, however, and this pattern no longer holds. They are shown in **n** for $C(CNHMe)NH_2$.

They may be described as a carbon lone pair σ and the three π orbitals of an "allylic" type N–C–N fragment. Only σ interacts with the frontier orbitals of the

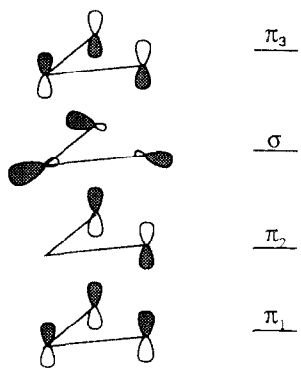

n

$MoCp_2Br^+$ fragment, d_π and d_σ, shown in **o**.

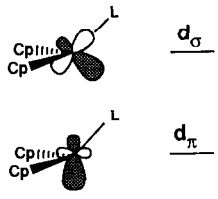

o

The π orbitals remain non-bonding, π_1 and π_2 both being occupied. The π bond is delocalized over the N–C–N atoms, but the two C–N bonds are non-equivalent due to the presence of only one Me group. This happens when the ligand lies in the Br–Mo–C or in any other plane, as only a σ bond is formed. The small preference found for the in-plane geometry may be due to less repulsion between the carbene ligand and the Cp rings.

The remaining question concerns the position of the methyl substituent (Scheme 3, **e**–**h**). As a complete geometry optimization is impossible, only the Br–Mo–C angle (α) was allowed to change. All the angles in the ligand were kept at 120°. Both **e** and **g** are equally stable ($\alpha = 90°$), while **f** and **h** are 0.7 and 6.1 eV (16 and 141 kcal mol^{-1}) higher in energy, respectively. The steric repulsion between Br and the adjacent methyl group is clearly responsible for the high energy of **h** (a geometry optimization would certainly lower this value), while in **f** there is smaller repulsion between this same methyl group and the Cp rings, analogous to what was found earlier for the C(NHMe)N(H)C(NHMe) ligand. The two most stable forms can be converted into each other by rotation around the M–C bond (Fig. 4).

The activation energy for rotation was found to be ~ 10 kcal mol^{-1} (0.45 eV), the transition state corresponding to a situation half through the rotation, when the methyl group approaches one of the Cp rings. In agreement with the qualitative bonding model described above, the M–C bond should be single, while both N–C bonds should be stronger than single bonds. The proposal that the two isomers **e** and **g** are those occurring in solution, with an easy interconversion, is thus feasible and is compatible with the available NMR data.

Conclusions

Mono(methylisocyanide) complexes of the type $[Cp_2M(X)CNMe]^+$ (M = Mo or W) can be readily prepared from the parent halide derivatives, but a di-cation, $\mathbf{3}^+$, could be obtained only in the case of Mo. The neutral complexes $[Cp_2MCNMe]$ (M = Mo or W) can also be prepared and, in contrast to the cationic complexes, show very extensive M-to-CNMe back-donation as judged from the ν(C≡NMe) values. The cations undergo nucleophilic addition reactions at the CNMe by CH_3O^-, PhS^-, NEt_3, or NH_3, to give cyclic and acyclic Fischer-type imino-carbene complexes. All these ligands lie on the plane bisecting the Cp–M–Cp angle and the reason for this preference in the acyclic complexes, was found to be mainly steric in origin. In fact, the lack of M–C double bond character is reflected on a rather low energy barrier for the rotation around the M–C bond, *ca.* 10 kcal mol^{-1}. However, the cyclic complexes, obtained by CH_3O^- or NH_3 addition to

3^+, already have some M–C multiple bond character as shown by EHMO calculations. The distortion observed in the solid state structure of $[Cp_2MoC\{N(H)CH_3\}N(H)C\{N(H)CH_3\}]^{2+}$, which can be viewed as an early stage of decyclization, can be interpreted as arising from asymmetries in the lattice, leading to unequal hydrogen bonds on both sides of the metallacycle. Borohydride addition to 3^+ follows a different course. EHMO calculations show that this regioselectivity results from either thermodynamic or kinetic orbital control. Both these types of regioselectivity had been observed before for Group 6 metallocene derivatives and illustrate the facility with which unsaturated ligand can be functionalized at the cationic Cp_2M moiety, a property that we intend to explore further.

Experimental

All preparations were carried out under an argon atmosphere using standard Schlenk techniques. All solvents were dried by refluxing over the appropriate reagents (CH_2Cl_2 and NCMe over CaH_2, THF, Et_2O, toluene and pentane over Na/benzophenone ketyl), distilled and stored under argon. NEt_3 was dried over Na_2SO_4 and distilled. $[Cp_2MX_2]$ [38], $[Cp_2MHI]$, [39], CNMe [40] were prepared according to literature methods and the other reagents were used as purchased. Elemental analyses were performed in our laboratories and in the Microanalytical Laboratory of the Anorganisch-Chemisches Institut der Technische Universität Munich, Germany. IR spectra (KBr) were run on a Perkin–Elmer 457 and on a Nicolet DX 5 FT (solution spectra). ^1H NMR spectra were recorded on a Jeol-JNM-100PFT, Bruker CXP-300 and Jeol-JMX-GX-400. $^{13}C\{^1H\}$ NMR spectra were recorded on the latter spectrometer. Chemical shifts were referenced to residual solvent signals. Mass spectra were obtained with a Finnigan MAT 311A spectrometer.

Preparations

$[Cp_2MoH(CNMe)]I$ (1). $[Cp_2MHI]$, (0.80 g, 2.26 mmol) and CNMe (139 μl, 2.95 mmol) in THF were heated under reflux for *ca.* 3 h, affording yellow crystals of **1** in quantitative yield, which were separated by filtration, washed with Et_2O and dried under vacuum. Anal. Found: C, 35.93; H, 3.51; N, 3.37. $C_{12}H_{14}INMo$ calc. (395.09): C, 36.48; H, 3.57; N, 3.55%.

$[Cp_2MoI(CNMe)]I$ (2). CHI_3 (0.41 g, 1.04 mmol) was added to a solution of $[Cp_2MoH(CNMe)]I$ (**1**) (0.41 g, 1.04 mmol) in CH_2Cl_2 and the mixture was allowed to react at room temperature for 2 h. Addition of Et_2O to the concentrated solution gave green crystals of **2** that were separated by filtration and dried under vacuum. The yield was quantitative.

Alternative preparation: addition of CNMe (35 μl, 0.74 mmol) to a suspension of $[Cp_2MoI_2]$ in acetonitrile (0.34 g, 0.71 mmol) followed by reflux for *ca.* 2 h, cooling to room temperature and addition of Et_2O, gives **2** also in quantitative yield. Anal. Found: C, 28.17; H, 2.62; N, 2.79. $C_{12}H_{13}I_2MoN$ calc. (520.99): C, 27.67; H, 2.51; N, 2.69.

$[Cp_2WBr(CNMe)]Br$ (4). CNMe (25 μl, 0.53 mmol) and $[Cp_2WBr_2]$ (0.17 g, 0.36 mmol) were heated under reflux in acetonitrile for 4 h affording an orange-brown solution. Concentration and addition of Et_2O gave brown crystals of **4** in

quantitative yield after filtration and drying under vacuum. Anal. Found: C, 27.39; H, 2.69; N, 2.73. $C_{12}H_{13}Br_2NW$ calc. (514.90): C, 27.99; H, 2.54; N, 2.72%.

*[$Cp_2Mo(CNMe)_2$]I_2 (**3a**).* A suspension of [Cp_2MoI_2] (0.39 g, 0.81 mmol) in *ca.* 40 ml of acetonitrile was treated with CNMe (150 μl, 3.18 mmol) and heated under reflux for 4 h. Upon cooling and addition of Et_2O yellow crystals of **3a** separated, and were filtered and dried in vacuum. Yield, 84%. Anal. Found: C, 30.24; H, 2.81; N, 4.97. $C_{14}H_{16}I_2MoN_2$ calc. (562.04): C, 29.92; H, 2.87; N, 4.98%.

*[$Cp_2Mo(CNMe)_2$]Cl_2 (**3b**).* Analogous to **3a**, from [Cp_2MoCl_2] (0.40 g, 1.34 mmol) and CNMe (200 μl, 4.24 mmol). Yield, 88%.

*[$Cp_2Mo(CNMe)_2$]$[PF_6]_2$ (**3c**).* To a solution of either **3a** or **3b** in acetonitrile was added excess $TlPF_6$. Immediately an abundant precipitate of TlX separated. After filtration and addition of Et_2O, yellow crystals of **3c** separated in 87% yield.

*[$CpMo(\eta^4\text{-}C_5H_6)(CNMe)_2$]$PF_6$ (**5**).* A solution of $NaBH_4$ (0.03 g, 0.79 mmol) in NCMe was added to a solution of **3c** (0.23 g; 0.39 mmol) in the same solvent. Some cloudiness developed and after 1.5 h at room temperature, the solution was filtered and concentrated. The yellow crystals formed were separated by filtration, washed with Et_2O and dried under vacuum. Yield, 80%. Anal. Found: C, 37.05; H, 3.72; N, 5.96; P, 6.85. $C_{14}H_{17}F_6MoN_2P$ calc. (454.20): C, 37.02; H, 3.77; N, 6.17; P, 6.82%.

*[$Cp_2\overline{MoC(OCH_3)N(CH_3)CNCH_3}$]$PF_6$ (**6**).* NaOMe (0.02 g, 0.36 mmol) in MeOH (5 ml) was added to a solution of **3c** (0.23 g, 0.36 mmol) in NCMe. The white precipitate formed was filtered off and the solution concentrated. On cooling to -50°C, yellow crystals of **6** formed. These were separated by filtration at low temperature, washed with Et_2O and dried under vacuum. Yield 85%. Anal. Found: C, 37.41; H, 4.15; N, 5.78. $C_{15}H_{19}F_6MoN_2P$ calc. (484.23): C, 37.21; H, 3.95; N, 5.79%.

[$Cp_2Mo(CNCH_3)\{C(SPh)N(H)CH_3\}$][$PF_6$]$_2$ (**7**). [Et_4N]SPh (0.06 g, 0.24 mmol) was dissolved in NCMe and added to a solution of **3c** (0.15 g, 0.24 mmol) in the same solvent. The mixture was allowed to react at room temperature for 1.5 h giving an orange solution. The solvent was then evaporated to dryness and the oily residue was repeatedly washed with Et_2O. The product was obtained after several recrystallizations of this residue from CH_2Cl_2/Et_2O.

*[$Cp_2Mo(CNCH_3)\{C(NEt_3)NCH_3\}$]$[PF_6]_2$ (**8**).* A solution of **3c** (0.19 g, 0.30 mmol) in NCMe was treated with 1 ml of NEt_3. After 4 h at room temperature, the solvent was evaporated and the solid residue washed with Et_2O. The product was recrystallized by slow diffusion of Et_2O into a CH_2Cl_2 solution of this residue. The yellow crystals formed were separated from the mother liquor by decantation *via* a cannula, washed with Et_2O and dried under vacuum. Yield, 75%. Anal. Found: C, 34.46; H, 4.43; N, 5.55; P, 8.88. $C_{20}H_{31}F_{12}MoN_3P$ calc. (699.35): C, 34.35; H, 4.47; N, 6.00; P, 8.86%.

*[$Cp_2\overline{MoC\{N(H)CH_3\}N(H)C\{N(H)CH_3\}}$]$[PF_6]_2 \cdot CH_3CN$ (**9**).* Dry gaseous NH_3 was bubbled through a solution of **3a** (0.10 g, 0.19 mmol) in NCMe for 1 h. Then, the Schlenk vessel was closed and the reaction left overnight. The addition of $TlPF_6$ (0.08 g, 0.23 mmol) to a well stirred solution led to the rapid precipitation of yellow TlI. This was filtered and the solution slowly evaporated under vacuum. The orange micro-crystals formed were filtered, washed with Et_2O and dried. Yield, 90%. Anal. Found: C, 29.32; H, 3.28; N, 8.36. $C_{16}H_{22}F_{12}MoN_4P_2$ calc. (656.24): C, 29.28; H, 3.38; N, 8.54.

[$Cp_2WBr\{C(NH_2)NHCH_3\}$]Br · CH_2Cl_2 (10). Dry gaseous NH_3 was bubbled through a solution of **4** (0.12 g, 0.23 mmol) in NCMe for 2 h. The Schlenk vessel was closed and left for 18 h at 30°C. The solvent was evaporated to dryness and the residue recrystallized from CH_2Cl_2/Et_2O. Yield, 80%. Anal. Found: C, 24.78; H, 3.02; N, 5.21. $C_{13}H_{18}Br_2Cl_2N_2W$ calc. (616.86): C, 25.31; H, 2.94; N, 4.54%.

[$Cp_2WBr(CHClPMe_3)$]Br · CH_2Cl_2 (11). PMe_3 (0.5 ml) was added to a solution of **4** (0.13 g, 0.25 mmol) in CH_2Cl_2. This mixture was left 10 h at room temperature and then the solvent was evaporated to dryness. After washing with Et_2O, the residue was taken in CH_2Cl_2. Slow addition of Et_2O gave colourless and orange crystals. Recrystallization at −20°C allowed the separation of both products. The colourless crystals were identified as [CH_2ClPMe_3]Cl and the orange crystals as **11** in 58% yield. Anal. Found: C, 27.56; H, 3.75; N, 2.07. $C_{17}H_{25}Br_2Cl_3NPW$ calc. (724.29): C, 28.19; H, 3.48; N, 1.93%.

[$Cp_2MoCNMe$] (12). A suspension of **1** (0.24 g, 0.61 mmol) in THF (40 ml) was treated with NaH (0.12 g, 5.0 mmol) with fast stirring at room temperature during 10 h. The reaction solution was filtered and the solvent evaporated. The resulting residue was extracted into Et_2O filtered and again evaporated to dryness. Sublimation onto a cold finger (tap water) at 65°C and 10^{-4} Torr gave **12** as a brown red crystalline solid. Best yield, 40%. Anal. Found: C, 53.55; H, 5.32; N, 4.84. $C_{12}H_{13}MoN$ calc. (267.18): C, 53.95; H, 4.90; N, 5.24%.

[Cp_2WCNMe] (13). Treatment of a suspension of **4** in THF (0.13 g, 0.25 mmol), with Na/Hg 1% (3.7 g, 1.59 mmol) at room temperature for 30 min gave a brown solution which was quickly filtered and evaporated to dryness. The residue was extracted with pentane until colourless extracts were obtained. The combined extracts were taken to dryness and the residue sublimed onto a cold-finger (65°C, 10^{-4} Torr) to give dark brown crystals. Best yield, 30%. EI-MS: m/z 355 (M^+), 314 ([M − CNMe]$^+$) (^{184}W).

*Crystal structure determination of **4** and **9***

*Crystal data for **4**.* The complex crystallizes in the triclinic space group $P\bar{1}$ with $a = 7.605(5)$, $b = 13.34(1)$, $c = 14.82(2)$ Å, $\alpha = 83.36(5)$, $\beta = 86.56(3)$, $\gamma = 79.77(4)°$, $V = 1468(2)$ Å^3, $F(000) = 944$, $Z = 4$ (with two independent molecules in the asymmetric unit), $\mu = 133.4$ cm^{-1}.

*Crystal data for **9**.* The complex crystallizes in the monoclinic space group $P2_1$ with $a = 9.754(9)$, $b = 11.175(9)$, $c = 10.008(7)$ Å, $\beta = 99.38(5)°$, $V = 1074(2)$ Å^3, $F(000) = 496$, $Z = 2$, $\mu = 6.0$ cm^{-1}.

Data collection. X-Ray intensity data were collected at room temperature with an Enraf–Nonius FAST area detector diffractometer using graphite monochromated Mo-K_α radiation ($\lambda = 0.71069$ Å) from a Nonius FR 571 rotating anode generator operating at 50 kV and 60 mA, with an apparent spot size of 0.3 × 0.3 mm^2. The intensity data measurements were carried out using SADNES, a modified version of MADNES [41] software for small molecule data collection.

For both data collections, the crystal to detector distance was set to 40 mm and a detector tilt angle of $\theta = 27°$ was used. In addition, an exposure time of 30 s per 0.40° frame (0.25° for **9**) was used throughout. In order to achieve a data set as complete as possible, eight (four for **9**) separate measurements were carried out, the details of which are given in Table 6 for **4** and Table 7 for **9**.

Table 6

Summary of intensity data measurements for the crystal of **4**

Datum angles ω, κ, ϕ [a]			Range of scan [b]		No. of observations measured	No. of unique reflections
180.00	0.00	0.00	−40.0	60.0	3253	3252
180.00	0.00	90.00	−40.0	60.0	3243	3243
167.01	39.49	−12.99	−38.0	60.0	3232	3231
167.01	39.49	61.03	−38.0	60.0	3208	3207
151.03	81.48	−28.97	−30.0	60.0	2955	2950
151.03	81.48	61.03	−30.0	60.0	2942	2941
122.97	134.73	−57.03	−27.5	42.5	2262	2262
122.97	134.73	32.97	−27.5	42.5	2240	2240

[a] Goniostat zero point for this measurement in kappa geometry. [b] The scan axis ϕ is parallel to the goniostat ω axis.

Reflection profiles were extracted on line from the integrated mass store images. Data reduction was later carried out by the Kabsch profile fitting method using the PROCOR program [42], which produced a file containing intensities corrected for Lorentz and polarization effects. The intensities from the independent measurements were then scaled and merged together with the SHELX-76 program [43].

For the $[Cp_2W(Br)(CNMe)]Br$ (**4**), a total of 23335 observations of 7911 independent reflections were measured and R_{merge} of 9.7% was obtained. This data set amounted to 84% of the theoretically predicted reflections in the resolution range 15.0 to 0.70 Å. For the crystal of $[Cp_2\overline{MoC\{N(H)CH_3\}N(H)C\{N(H)CH_3\}}][BF_4]_2 \cdot CH_3CN$ (**9**), a total of 7462 observations of 3140 independent reflections were measured and an R_{merge} of 3.1% was obtained. This data set amounted to 87% of the theoretically predicted in the resolution range 7.52–0.70 Å.

The initial values of the cell parameters were determined by an auto indexing procedure applied to 50 intense reflections covering two narrow (*ca.* 5° wide) and nearly orthogonal regions of reciprocal space. Throughout the data collection process, the cell parameters were refined together with the orientation matrix every 12° (10° for **9**) of measured data using the positions of the most recently measured 250 strong reflections. The values used in the structure determination

Table 7

Summary of intensity data measurements for the crystal of **9**

Datum angles ω, κ, ϕ [a]			Range of scan [b]		No. of observations measured	No. of unique reflections
180.00	0.00	0.00	−60.0	40.0	2266	1584
180.00	0.00	90.00	−60.0	40.0	2075	1620
151.03	81.48	−28.97	−27.5	45.5	1598	1567
151.03	81.48	61.03	−27.5	45.5	1523	993

[a] Goniostat zero point for this measurement in kappa geometry. [b] The scan axis ϕ is parallel to the goniostat ω axis.

and refinement and their reported e.s.d.s were obtained from the mean and s.d. values computed from the refined values of the cell parameters which were based on more than 150 intense reflections.

Structure solution and refinement. Both structures were solved by a combination of Patterson and Fourier methods and refined by full matrix least-squares. Following convergence of the isotropic refinement, the observed structure factor data were corrected for absorption using the DIFABS program [44] modified for the FAST geometry. This procedure lowered the *R*-factor from 17.5% to 13.7% for all the 6655 unique reflections. The W and some of the Br atoms were refined anisotropically and refinement was carried out to convergence with SHELX-76 [43]. No hydrogen atoms were located in the difference electron density map and none

Table 8

Fractional atomic coordinates ($\times 10^4$) for complex **4**

	x	y	z
W(1)	11530(1)	2230(1)	4133(1)
W(2)	4530(1)	2966(1)	8151(1)
Br(1)[a]	9280(3)	1722(2)	5435(2)
Br(2)	5064(4)	1225(2)	7446(2)
Br(3)	5000	5000	5000
Br(4)	0	0	0
Br(5)	6071(4)	3068(2)	1685(2)
C(11)	10305(29)	1379(19)	3419(16)
N(11)	9662(26)	882(16)	3002(14)
C(12)	8906(37)	230(23)	2467(20)
C(21)	4401(29)	2032(19)	9317(17)
N(21)	4286(26)	1831(17)	10006(15)
C(22)	4316(34)	881(22)	10895(19)
C(31)	9391(39)	3376(25)	3389(22)
C(32)	9446(35)	3756(22)	4210(19)
C(33)	11113(40)	3952(25)	4289(21)
C(34)	12058(37)	3735(23)	5410(20)
C(35)	10998(43)	3385(25)	2938(23)
C(41)	13404(34)	1189(21)	5182(18)
C(42)	14270(36)	2021(23)	4849(20)
C(43)	14601(34)	1988(21)	3920(19)
C(44)	14025(33)	1135(21)	3673(18)
C(45)	13123(33)	650(20)	4406(18)
C(51)	1748(40)	3689(26)	8703(22)
C(52)	1569(38)	2841(25)	8284(22)
C(53)	1923(42)	3026(26)	7360(23)
C(54)	2504(38)	3921(25)	7168(21)
C(55)	2443(47)	4408(29)	8026(25)
C(61)	6646(39)	3472(20)	8957(17)
C(62)	6195(33)	4238(21)	8227(18)
C(63)	6818(39)	3726(25)	7405(21)
C(64)	7508(33)	2806(21)	7623(18)
C(65)	7445(34)	2579(21)	8569(19)
Br(4')	10011(33)	2288(21)	10693(18)
Br(5')	1905(67)	4060(41)	7a2(36)

[a] The d.o.f. of the Br sites are, respectively: 0.42 for atom Br(4) and 0.08 for atom Br(4'); 0.91 for atom Br(5) and 0.09 for atom Br(5').

were introduced in idealized positions. At this point there were still some peaks in the difference electron density map, which were assigned as disordered positions of the Br counter ions. Final R values of 6.3% and R_w of 8.5%, for 2272 reflections ($F \geq 2\sigma F$) and 172 refined parameters, were obtained using a weighting scheme of the form $[w = 1.0/(\sigma^2 F + 0.0063F^2)]$. The highest residual electron density in the final difference map was 2.9 e Å^{-3} near the positions of the W atoms.

For complex **9**, systematic absences agreed with space groups $P2_1$ or $P2_1/m$. Refinement was tried in $P2_1/m$ with the fragment MoC1N1C2N2N3 in the mirror plane, but it was not successful, giving unreasonable geometric parameters for the fragment. The structure was then solved and refined in $P2_1$. The isotropic agreement factor was 15.1%. One of the Cp rings was found to have some disorder

Table 9

Fractional atomic coordinates ($\times 10^4$) for complex **9**

	x	y	z
Mo	1992(2)	2500	2143(2)
N(1)	2495(14)	2381(25)	4895(13)
N(2)	4769(15)	2498(35)	4413(15)
N(3)	50(15)	2499(37)	4486(16)
C(1)	3536(19)	2584(27)	3919(17)
C(2)	1264(18)	2552(31)	4027(17)
C(3)	5550(22)	2676(28)	5822(22)
C(4)	−116(26)	2510(47)	5965(20)
N(20)	8337(24)	2518(43)	8585(23)
C(21)	7350(26)	2509(45)	−925(19)
C(22)	6089(28)	2482(67)	−324(32)
B(1)	6988(30)	4674(27)	3666(35)
F(11)	6346(67)	5390(71)	2592(58)
F(12)	7150(54)	3659(37)	2878(58)
F(13)	7318(95)	5170(99)	2444(38)
F(14)	8366(27)	4768(38)	3445(77)
B(2)	7077(21)	135(19)	3073(21)
F(21)	8188(44)	41(36)	4091(33)
F(22)	6174(43)	693(66)	2083(50)
F(23)	6286(21)	104(18)	4115(17)
F(24)	7205(48)	−1026(20)	2583(24)
C(31)	435(41)	1164(46)	1443(39)
C(31′)	704(42)	765(39)	1484(32)
C(32)	1094(53)	565(42)	2637(40)
C(32′)	1651(49)	457(38)	2655(33)
C(33)	2512(50)	424(46)	2443(48)
C(33′)	2870(37)	593(36)	2032(46)
C(34)	2857(41)	733(46)	1148(55)
C(34′)	2581(38)	1097(40)	691(39)
C(35)	1458(41)	1021(45)	582(48)
C(35′)	1126(40)	1333(38)	339(35)
C(41)	1772(28)	3732(30)	343(27)
C(42)	3041(29)	4009(29)	1210(30)
C(43)	2872(27)	4451(32)	2526(31)
C(44)	1367(27)	4433(30)	2291(27)
C(45)	635(27)	3989(30)	1036(27)

and a model with 70% and 30% occupancy factors could be fitted. The other Cp ring was refined isotropically, the atomic displacement parameters indicating large thermal motion. The Cp rings were refined with fixed C–C distances (1.42 Å). The C1N1C2N2N3 ligand and the BF_4^- anions were refined anisotropically. A restrained model of the BF_4^- was used in the refinement (B–F, 1.40 Å). Final refinement converged to an R of 10.7%, R_w of 10.0% for 1563 reflections ($F \geq \sigma F$) and 237 refined parameters, using unit weights ($w = 1.0/\sigma^2 F$). Due to the poor quality of the crystal, a limited number of non-zero data limited the precision of the model obtained. As in complex **4**, no H atoms were found in the difference electron density map and none were introduced in idealized positions. The highest residual electron density in the final difference map was 0.75 e Å^{-3}.

Atomic scattering factors were taken from International Tables [45]. Final atomic positional parameters for the non-hydrogen atoms are presented in Tables 8 and 9. Anisotropic and isotropic thermal motion parameters, calculated hydrogen parameters and coefficients of selected least-squares planes are given as supplementary material. Lists of observed and calculated structure factors for both complexes are available from the authors.

Extended Hückel molecular orbital calculations. All calculations were of the extended Hückel type [13] with modified H_{ij}'s [46]. The basis set for the metal atoms consisted of *ns*, *np*, and $(n-1)d$ orbitals. The *s* and *p* orbitals were described by single Slater-type wave functions, and the *d* orbitals were taken as contracted linear combinations of two Slater-type wave functions.

The geometry of $[Cp_2MoC\{N(H)CH_3\}N(H)C\{N(H)CH_3\}]^{2+}$ was taken from the structure described in this work, assuming the complex to have C_{2v} symmetry. Distances (Å) and angles (°) were the following: Mo–Cp 2.00; C–C 1.40; C–H 1.08; C–N 1.46; N–H 1.02; Cp–Mo–Cp 132; C–Mo–C 64; all angles inside the ligand were 120° (except those in the four-membered cycle). The iron complex was modelled after the structure in [18b] for $[Fe(CNMe)_4\{C(NHMe)N(Me)C(NHMe)\}]^{2+}$ keeping the ligand as before. The same basic geometry, in accordance with that found in $[Pt\{C(NHMe)_2\}_4][PF_6]$ [47], was used in the carbene ligand $C(NHMe)(NH_2)$ in the complex $[MoCp_2(Br)\{C(NHMe)(NH_2)\}]^+$, the Mo–Br distance being 2.60 Å. The C–Mo–Br angle was optimized as mentioned in the text.

Standard parameters were used for C, N, and H. Those for Mo and Br were the following (orbital, H_{ii}/eV, ζ): Mo 5*s* −8.77, 1.96; Mo 5*p* −5.60, 1.90; Mo 4*d* −11.06, 4.54, 1.90 (ζ_2), 0.5899 (C_1), 0.5899 (C_2); Br 4*s* −25.0, 2.64; Br 4*p* −13.1, 2.26.

The three-dimensional plot in **d** was done using the CACAO program [48].

Acknowledgements

We thank Professor W.A. Herrmann of the Technische Universität München and his group for receiving A.M.M. and providing analytical and spectroscopic facilities. In particular, we thank Dr. A. Filippou for his guidance and for helpful discussions. This work was partially funded by Junta Nacional de Investigação Científica and Tecnológica (PMCT/C/CEN/367/90), Instituto Nacional de Investigação Científica and Instituto Superior Técnico. A.M.M. thanks the Gulbenkian Foundation for a grant.

References

1 R. Davis and L.A.P. Kane-Maguire, in G. Wilkinson, F.G.A. Stone and E.W. Abel (Eds.), Comprehensive Organometallic Chemistry, Vol. 3, Pergamon Press, Oxford 1982, pp. 1149 and 1321.

2 (a) K.L.T. Wong, J.L. Thomas and H.H. Brintzinger, J. Am. Chem. Soc., 96 (1974) 3694; (b) F.W.S. Benfield and M.L.H. Green, J. Chem. Soc., Dalton Trans., (1974) 1324; (c) J.L. Thomas, Inorg. Chem., 17 (1978) 1507; (d) G.L. Geoffroy and M.G. Bradley, Inorg. Chem., 17 (1978) 2410; (e) T.C. Wright, G. Wilkinson, M. Motevalli and M.B. Hursthouse, J. Chem. Soc., Dalton Trans., (1986) 2017; (f) C.G. de Azevedo, A.R. Dias, A.M. Martins and C.C. Romão, J. Organomet. Chem., 363 (1989) 57; (g) M.J. Calhorda, M.A.A.F. de C.T. Carrondo, A.R. Dias, A.M.T. Domingos, M.T.L.S. Duarte, M.H. Garcia and C.C. Romão, J. Organomet. Chem., 320 (1987) 63; (h) F.W.S. Benfield and M.L.H. Green, J. Chem. Soc., Dalton Trans. (1974) 1244; (i) M.J. Calhorda and A.R. Dias, J. Chem. Soc., Dalton Trans., (1980) 1443.

3 M.J. Calhorda, A.R. Dias, A.M. Martins and C.C. Romão, Polyhedron, 8 (1989) 1802.

4 A.M. Martins, M.J. Calhorda, C.C. Romão, C. Völkl, P. Kiprof and A.C. Filippou, J. Organomet. Chem., 423 (1992) 367.

5 (a) A.C. Filippou, W. Grünleitner, E. Herdtweck, J. Organomet. Chem., 373 (1989) 325; (b) M. Novotny and S.J. Lippard, Inorg. Chem., 13 (1974) 828.

6 L.M. Jackman and S. Sternhall, Applications of Nuclear Magnetic Resonance Spectroscopy in Organic Chemistry, 2nd edition, Pergamon Press, Oxford, 1969, p. 164.

7 B. Crociani and R.L. Richards, J. Organomet. Chem., 144 (1978) 85.

8 T. Aviles, M.L.H. Green, A.R. Dias and C.C. Romão, J. Chem. Soc., Dalton Trans., (1979) 1367.

9 (a) N.J. Cooper and M.L.H. Green, J. Chem. Soc., Chem. Commun., (1974) 761; (b) M. Ephritikine, B.R. Francis, M.L.H. Green, R.E. Mckenzie and M.J. Smith, J. Chem. Soc., Dalton Trans., (1977) 1131.

10 S.G. Davies, S.D. Moon, S.J. Simpson and S.E. Thomas, J. Chem. Soc., Dalton Trans., (1983) 1805.

11 C.G. Kreiter, J. Kögler and K. Nist, J. Organomet. Chem., 310 (1986) 35.

12 C.G. de Azevado, M.A.A.F. de C.T. Carrondo, A.R. Dias, M.T. Duarte, M.F.M. Pledade and C.C. Romão, in preparation.

13 (a) R. Hoffmann, J. Chem. Phys. 39 (1963) 1397; (b) R. Hoffmann and W.N. Lipscomb, J. Chem. Phys., 36 (1962) 2179.

14 V. Riera and J. Ruiz, J. Organomet. Chem., 384 (1990) 339.

15 W. Kemp, NMR in Chemistry: A Multinuclear Introduction, Macmillan, London, 1986, p. 74.

16 E. Breitmaier and W. Voelter, Carbon-13 NMR Spectroscopy: High Resolution Methods and Applications in Organic Chemistry and Biochemistry, 3th edition, VCH Verlagsgesellschaft, D-6940 Weinheim, 1987.

17 P. Jernakoff and N.J. Cooper, J. Am. Chem. Soc., 111 (1989) 7424.

18 (a) D.J. Doonan and A.L. Balch, Inorg. Chem., 13 (1974) 921; (b) J. Miller, A.L. Balch and J.H. Enemark, J. Am. Chem. Soc., 93 (1971) 4613.

19 A.L. Steimetz and B.W. Johnson, Organometallics, 2 (1983) 705.

20 P.R. Branson, R.A. Cable, M. Green and M.K. Lloyd, J. Chem. Soc., Dalton Trans., (1976) 12.

21 W. Hummel, J. Hauser and H.-B. Bürgi, PEANUT, Computer Graphics Program to Represent Atomic Displacement Parameters, J. Mol. Graphics, 8 (1990) 214.

22 (a) K. Prout, T.S. Cameron, R.A. Forder, S.R. Critchley, B. Denton and G.V. Rees, Acta Crystallogr., Sect. B, 30 (1974) 2290; (b) M.J. Calhorda and A.M. Galvão, Bonding and conformations in biscyclopentadienylthiolate derivatives of early transition metals, in Topics in Physical Organometallic Chemistry, Vol. 4, Freund Publishing, Tel-Aviv, 1991.

23 C.T. Lam, D.L. Lewis and S.J. Lippard, Inorg. Chem., 15 (1976) 989.

24 A.G. Orpen, L. Brammer, F.H. Allen, O. Kennard, D.G. Watson and R. Taylor, J. Chem. Soc., Dalton Trans., S1, 1989.

25 M.-K. Lee, P.S. Huang, Y.S. Wen and J.T. Lin, Organometallics, 9 (1990) 2181.

26 J.L. Davidson, W.F. Wilson and K.W. Muir, J. Chem. Soc., Chem. Commun., (1985) 460.

27 A.J. Schultz, K.M. Stearley, J.M. Williams, R. Mink and G.D. Stucky, Inorg. Chem., 16 (1977) 3303.

28 A.N. Protski, B.M. Bulychev, G.L. Soloveichik and V.K. Belsky, Inorg, Chim. Acta, 115 (1986) 121.

29 M.J. Calhorda, M.A.A.F. de C.T. Carrondo, R. Gomes da Costa, A.R. Dias, M.T.L.S. Duarte and M.B. Hursthouse, J. Organomet. Chem., 320 (1987) 53.

30 R.S. Pilato, C.E. Housmekerides, P. Jernakoff, D. Rubin, G.L. Geoffroy and A.L. Rheingold, Organometallics, 9 (1990) 2333.
31 M.A.A.F. de C.T. Carrondo, A.R. Dias, M.H. Garcia, A. Mirpuri, M.F.M. Piedade and M.S. Salema, Polyhedron, 8 (1989) 2439.
32 M.J. Calhorda, M.A.A.F. de C.T. Carrondo, A.R. Dias, A.M.T.S. Domingos, J.A. Martinho Simões and C. Teixeira, Organometallics, 5 (1986) 660.
33 M.A.A.F. de C.T. Carrondo and V. Félix, in preparation.
34 M.J. Calhorda, M.A.A.F. de C.T. Carrondo, A.R. Dias, A.M. Galvão, M.H. Garcia, A.M. Martins, M.E. Minas de Piedade, C.I. Pinheiro, C.C. Romão, J.A. Martinho Simões and L.F. Veiros, Organometallics, 10 (1991) 483.
35 C.G. de Azevedo, M.J. Calhorda, M.A.A.F. de C.T. Carrondo, A.R. Dias, V. Félix and C.C. Romão, J. Organomet. Chem., 391 (1990) 345.
36 (a) J.W. Lauher and R. Hoffmann, J. Am. Chem. Soc., 98 (1976) 1729; (b) R.J. Goddard and R. Hoffmann, *ibid.*, 102 (1980) 7667.
37 M.J. Calhorda, M.A.A.F. de C.T. Carrondo, A.R. Dias, C.F. Frazão, M.B. Hursthouse, J.A. Martinho Simões and C. Teixeira, Inorg. Chem., 27 (1988) 2513.
38 R.L. Cooper and M.L.H. Green, J. Chem. Soc. A, (1967) 1155.
39 P. Grebenik, Part II. Thesis, Oxford, 1974.
40 R.E. Schuster, J.E. Scott and J. Casanova Jr., Org. Synth. Coll., 5 (1973) 772.
41 (a) A. Messerschmidt and J.W. Pflugrath, Crystallography in Molecular Biology, Meeting Abstracts, Bischenberg, France, 1985; (b) A. Messerschmidt and J.W. Pflugrath, J. Appl. Crystallogr., 20 (1987) 306.
42 W. Kabsch, J. Appl. Crystallogr., 21 (1988) 916.
43 G.M. Sheldrick, SHELX, Crystallographic Calculation Program, University of Cambridge, 1976.
44 N. Walker and D. Stuart, DIFABS, Acta Crystallogr., Sect. A39 (1983) 158.
45 T. Hahn (Ed.), International Tables for Crystallography, Vol. A, D. Reidel, Dordrecht, 1983.
46 J.H. Ammeter, H.-B. Bürgi, J.C. Thibeault and R. Hoffmann, J. Am. Chem. Soc., 100 (1978) 3686.
47 S.Z. Goldberg, R. Eisenberg and J.S. Miller, Inorg. Chem., 16 (1977) 1502.
48 C. Mealli and D.M. Proserpio, J. Chem. Ed., 66 (1990) 399.